Structural, electronic, and magnetic features of platinum alloy strings templated on a boron-doped carbon nanotube

Wei An and C. Heath Turner*
Department of Chemical and Biological Engineering, The University of Alabama, P.O. Box 870203, Tuscaloosa, Alabama 35487-0203, USA
(Received 15 October 2009; revised manuscript received 5 April 2010; published 25 May 2010)

We present density-functional-theory calculations of structural, electronic, and magnetic properties of platinum-alloy strings templated on a boron-doped single-wall carbon nanotube (6,6) model, B-SWCNT(6,6). Our calculations show that the alloy strings demonstrate strong molecular recognition, forming well-defined covalent bonds with the substrate and lead to the self-assembly of stable monatomic chains. The electronic and magnetic features of the Pt-alloy string/B-SWCNT(6,6) composite systems are mainly controlled by the presence of a magnetic alloying element (i.e., Fe, Co, and Ru). By changing the composition of the Pt alloy, the easy magnetization axis of the system can oscillate between the directions parallel and perpendicular to the tube axis. Our studies suggest that pure transition-metal (TM) or TM-alloy strings anchored on a substrate via strong molecular interactions can still possess sizable magnetic anisotropy due to spin-orbital coupling effects.

DOI: 10.1103/PhysRevB.81.205433 PACS number(s): 71.15.Mb

I. INTRODUCTION

As a one-dimensional (1D) material, carbon nanotubes (CNTs) have demonstrated remarkable versatility and wide applicability in emerging nanotechnologies,[1–3] such as components in field-effect transistors, optoelectronics, and spintronic devices. In parallel, the unusual electronic and magnetic properties of 1D transition-metal (TM) systems have also attracted considerable research interest from both experimentalists[4–9] and theoreticians.[10–36] For instance, intriguing phenomena, such as spontaneous spin-polarized transport[8] and quantum ballistic anisotropic magnetoresistance,[10] have been observed in 1D TM nanowires having strong magnetic anisotropy. Unfortunately, there is a great deal of important information about the fundamental magnetic and electrical properties of low-dimensional materials that still remains unknown.

Magnetic anisotropy originates primarily from the orbital magnetization via spin-orbit coupling (SOC) between the spins and the lattice of the material, which introduces preferential magnetization from one crystallographic direction to another, i.e., magnetocrystalline anisotropy. In bulk TMs, magnetic anisotropy is typically very weak. The orbital magnetic moments are quenched by strong crystal-field splitting and the hybridization of the *d* orbitals with that of neighboring atoms, and the spin-magnetic moments are substantially reduced by the large kinetic energies of the electrons at finite temperature. These contributions result in nonmagnetic ground states for most TMs. By contrast, in low-dimensional TM systems (e.g., 1D TM nanowires), Hund's rule is manifested by the reduced coordination of the atomic sites, giving rise to enhanced spin- and orbital-magnetic moments. Thus, strong magnetic anisotropy is most likely to be found from low-dimensional TM structures at nanometer length scales since there is an intrinsic tendency of the magnetization to align along the easy axis at zero magnetic field. Examples include monatomic chains of Ru, Rh, and Pd,[13] Os, Ir, and Pt,[16] Fe,[18] and Ni,[10] as well as Fe monatomic chains deposited on a Au (Ref. 6) or Cu (Refs. 32 and 33) substrate, and Co chains deposited on a Pt (Refs. 4, 5, 22–24, 27, 31, and 37) or Pd (Ref. 26) substrate. Advanced experimental techniques have made it possible to prepare these novel, low-dimensional TM nanostructures and simultaneously probe their structural, electronic, and magnetic properties at the atomic level.[4–9]

Compared to their bulk counterparts, freestanding 1D TM nanowires are energetically less stable with respect to thermal fluctuations, which can destroy their long-range magnetic order in the absence of an external magnetic field. For this reason, the giant magnetic anisotropy of isolated 1D TM nanowires predicted by theoretical studies is unlikely to be achieved in a real system. Therefore, for any future applications, it is critical for 1D TM nanowires to be stabilized on an appropriate substrate, which would maintain the fundamental electrical and magnetic features of these systems.

Our recent studies[38] have shown that TM strings templated on boron-doped single-walled carbon nanotubes (B-CNTs) demonstrate strong molecular recognition, leading to the self-assembly of TM atoms with well-defined covalent bonds with the substrate. Such B-CNT-templated TM strings exhibit high stability and unexpected electronic properties. These promising results have prompted further investigations into the structural, electronic, and magnetic features of TM-*alloy* monatomic chains anchored on B-CNTs.

Monatomic chains, composed of TM alloys, have also been a subject of active research since there exists a great deal of electronic and magnetic tuneability that can be achieved on very small length scales.[39–43] For instance, a previous study showed that the quantized conductance in AuPd and AuAg alloy nanocontacts can be modified by the alloying element in Au.[42] Very recently, suspended alloy monatomic chains have been experimentally realized by mechanically stretching a binary alloy $Au_{1-x}Ag_x$ (x=0.2, 0.4, 0.6, and 0.8) (Ref. 40) and this success sheds light on the potential synthesis of other monatomic TM-alloy chains.

II. COMPUTATIONAL METHODS

Our density-functional-theory (DFT) calculations were carried out using the Vienna *ab initio* simulation package

(VASP).[44,45] The models and computational details have been described elsewhere.[38,46] Particularly, spin-polarized DFT with projector augmented wave potentials,[47] the generalized gradient approximation Perdew, Burke, and Ernzerhof (PBE) functional,[48] and a plane-wave-base set with an energy cutoff of 400 eV were employed for all of the calculations. Three unit cells of B-SWCNT(6,6) along the tube's c axis were included to build the hexagonal supercell with $a=b=22$ Å in the other two directions of the tube. These dimensions are sufficiently large to avoid the interactions between the tube and its periodic images. The Brillouin zone of the supercell was sampled by $1\times1\times5$ k points within the Monkhorst-Pack scheme in structural optimization and first-order Methfessel-Paxton smearing[49] of 0.2 eV was used in the integration. The initial configurations were arranged in such a fashion that the interaction between the B-CNTs and the Pt-alloy chains are to be maximized. Consistent with our previous study of pure monatomic chains,[38] we aligned the chain axis with the tube axis (atop the B-doped sites) with a separation distance of 3 Å. All atom positions in the supercell were fully relaxed using the conjugate-gradient algorithm and the convergence threshold was set to be 10^{-4} eV for the total energy and 10^{-2} eV/Å in force on each atom. Only the lowest-energy configurations are presented in this work. The density of states (DOS) was calculated using $1\times1\times10$ k points based on the optimized structures. The binding energies (BEs) between the Pt-alloy strings and the B-SWCNT(6,6) (tube) is defined as $BE=(E_{total}[\text{tube+TM-string}]-E_{total}[\text{tube}]-E_{total}[\text{TM-string}])/n$, where E_{total} and n are the total energy of the system and the number of metal atoms per supercell, respectively. The relativistic effects of the third-row heavy-metal Pt is taken into account by performing fully relativistic calculations of the core electrons and a scalar-relativistic approximation for the valence electrons, as implemented in the default mode of VASP.

Furthermore, we calculated the magnetic anisotropy using noncollinear DFT (including SOC effects)[45,50] by aligning the spin-quantization axis parallel to and perpendicular to the tube axis. The magnetic anisotropy energy (MAE) is defined as the difference in total energies from self-consistent calculations for parallel and perpendicular direction of the magnetic axis, i.e., $MAE=E_{total}[\perp]-E_{total}[\parallel]$, where $E_{total}[\perp]$ and $E_{total}[\parallel]$ are the total energy of the system per supercell with magnetization directions to be perpendicular ($\perp$) and parallel ($\parallel$) to the tube axis, respectively (see Fig. 1). Thus, positive (negative) values of MAE correspond to the parallel (perpendicular) easy magnetization axes. Note that the magnetocrystalline anisotropy, which is the primary contribution to magnetic anisotropy, is taken into account by our electronic-structure calculations. However, the shape anisotropy arising from magnetostatic effects, i.e., the magnetic dipolar interaction, is not included in our calculations.

III. RESULTS AND DISCUSSION

The justifications of the models used in this study have been detailed elsewhere.[38] In this work, we mainly focus on a B-SWCNT(6,6) model, with boron doped in a locally concentrated fashion. This dopant arrangement is more likely to stabilize the linear chain structures, as shown in Fig. 2. Although the experimental realization of these exact structures is unclear, our study is intended to establish a benchmark for the properties of these composite structures, including the lowest limit for the MAE. Since previous experimental groups have synthesized (separately) TM monatomic chains[4–9] and B-doped CNTs,[51,52] it is plausible that some similar composite systems could eventually be realized. Here, we simply refer to this substrate model throughout the text as B-CNT since there are no other diameters or doping patterns investigated in the present study.

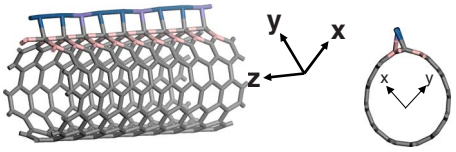

FIG. 1. (Color online) Diagram of the magnetization directions along x[100], y[010], and z[001], respectively. The z direction is parallel to the tube axis while the x and y directions are perpendicular to the tube axis. The gray color represents carbon, pink represents boron, and the other species correspond to a representative TM-alloy-string. A larger supercell is presented in the figure to help guide the readers' eye.

A. Structural features

Several studies of TM monatomic chains supported on Pt substrates have been previously reported.[4,5,7,11,21–24,27] For example, Gambardella *et al.*[4] revealed the existence of both short- and long-range ferromagnetic orders at 45 K for 1D Co chain segments constructed on the steps of the vicinal Pt(997) surface. Dallmeyer *et al.*[7] observed monatomic Co and Cu chain grown by step decoration of the vicinal Pt(997) surface and the presence of a 1D exchange-split band, and the presence of local magnetic moments. Rodrigues *et al.* prepared suspended Co, Pd, and Pt atomic chains using mechanically controlled break-junction methods, and provided certain experimental evidence for their spin-polarized conduction.[8] Although, the presence of impurities may have been an influencing factor.

Our calculations show that pure Fe, Co, and Ru monatomic chains retain most of their magnetic moments after anchored on B-CNT, i.e., $\mu_0=3.09$ and $\mu=2.62\mu_B$/Fe atom, $\mu_0=1.76$ and $\mu=1.33\mu_B$/Co atom, and $\mu_0=1.12$ and $\mu=1.08\mu_B$/Ru atom, respectively, as shown Table I. Thus, in this study, Fe, Co, and Ru were selected to create binary Pt-alloy chains with different compositions. In these models, alloy chains with the formula Pt_2M, PtM, and PtM_2 were tested (where M=Fe, Co, and Ru), and we investigated the alloying effects on the electronic and magnetic properties of the TM-alloy-string/B-CNT composite materials.

As shown in Fig. 2, the Pt-alloy-strings templated on B-CNT demonstrate strong molecular recognition, forming well-defined covalent bonds with the substrate (see BEs in Table I) and lead to the self-assembly of stable monatomic chains. These interactions are consistent with our recent studies of pure TM strings on B-CNT substrates.[38] The BEs of the Pt-alloy chains on the B-CNT range from −1.34 to

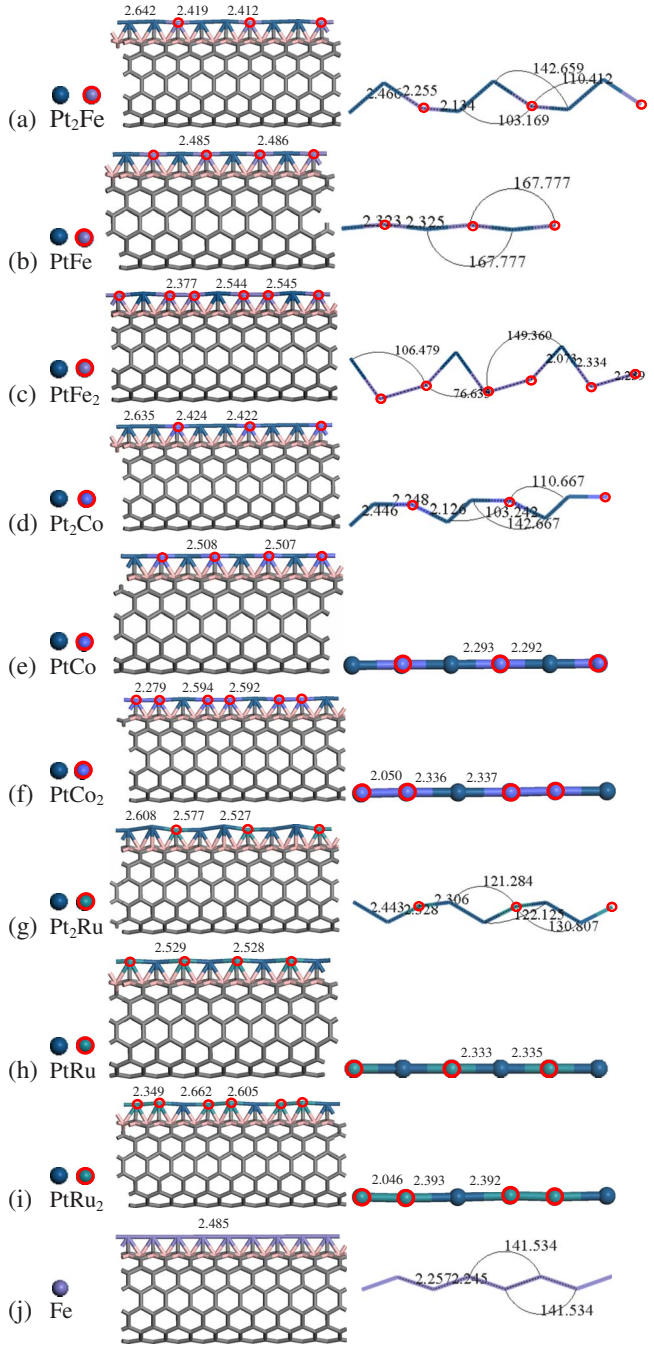

FIG. 2. (Color online) Side view of the TM-alloy string/B-SWCNT(6,6) and isolated monatomic TM-alloy chains. Equilibrium TM-TM bond length (Å) and angles (°) are labeled. Carbon atoms are shown in gray and boron atoms are shown in pink. A larger supercell is shown to help guide the eye.

−1.99 eV, and these values are similar to those of pure TM chains (BE=−1.70 eV, −1.75 eV, −1.45 eV, and −1.93 eV for Pt, Fe, Co, and Ru, respectively). The binding nature of the binary Pt-alloy-strings on the B-CNT can be identified as chemisorption, as evidenced by the formation of multiple TM-C and TM-B bonds, as well as the short binding distances (BDs), as seen in Table I.

The isolated Pt-alloy chains studied in this work adopt either a zigzag (Pt_2Fe, PtFe, $PtFe_2$, Pt_2Co, and Pt_2Ru) or quasilinear (PtCo, $PtCo_2$, PtRu, and $PtRu_2$) structure under a zero-strain condition. This is in contrast to the pure TM monatomic chains, which predominantly adopt zigzag configurations. After anchored on top of the B-CNT adsorbent, the equilibrium structures of the chains are reconstructed to match the lattice parameter of B-CNT, forming a continuous stringlike geometry. This suggests that the self-assembly phenomena of TM atoms deposited on B-CNTs is a general feature, regardless of the TM composition (pure or alloy). Undoubtedly, the enhanced binding strength of the B-CNT plays a key role in such atomic reconstruction since this behavior cannot be reproduced on a pristine CNT model. The underlying chemical binding trends should also hold for larger single-walled or multiwalled B-CNTs, which contain similar levels of boron.

B. Electronic and magnetic features

The calculated total density of states (TDOS) and projected-DOS (PDOS) for the Pt-alloy-string/B-CNT composite materials are displayed in Fig. 3. It can be seen that all of these systems remain magnetic, though the formation of multiple TM-C and TM-B bonds generally leads to reduced magnetic moments, as compared to those of pristine Pt-alloy monatomic chains (see Table I). As two extreme cases, gas-phase TM atoms possess the maximum spin- (μ_S) and orbital- (μ_L) magnetic moments, which is solely mediated by the intra-atomic Coulomb interactions. In stark contrast, the μ_S and μ_L for a three-dimensional bulk structure are partially or even totally quenched due to electron delocalization and crystal-field effects. Essentially, the 1D freestanding TM monatomic chains and their deposited structures retain a large fraction of their magnetic moment due to their reduced dimensionality.

As mentioned in Sec. I, the magnetic anisotropy is a critical parameter when considering the applicability of a material for a magnetic or spintronic device. The MAE serves as an energy barrier which represents the stability of the magnetization aligning along a specific spatial direction, and without a high barrier, the magnetic properties can be compromised by stochastic thermal fluctuations in the material. For simplicity and for maintaining a reasonable computational cost, most previous theoretical studies of the magnetic anisotropy of TM systems have been performed on freestanding monatomic chains[10–20,25,28–30] and on single TM atoms or finite monatomic chains deposited on a substrate.[11,21,23,26,27,31–33] Such calculations are able to provide the maximum possible magnetic anisotropy for TM structures deposited on substrates via weak molecular interactions. However, in reality, the components of an actual magnetic or spintronics device would need to be connected by well-defined bonding, if reliable performance is to be expected. Hence, there are several questions that must be addressed in order to obtain preliminary indications of performance, following device integration: (1) can the magnetic anisotropy survive after establishing well-defined interactions between the TM and the substrate? and (2) if so, how does the magnetic anisotropy evolve?

In order to address these questions, we performed computationally expensive calculations on the magnetic anisotropy

TABLE I. Calculated BE (in eV/TM atom), BD (in Å), magnetic anisotropy energy (MAE, in meV/TM atom), and spin- and orbital-magnetic moments (μ, in μ_B/TM atom) for TM-alloy-string/B-CNT systems.

	BE	BD (Bond)[a]	MAE	$\mu_{S\|\|}$	$\mu_{L\|\|}$	$\mu_{S\perp}$	$\mu_{L\perp}$	μ [b]	μ_0
Pt	−1.70	2.007 (Pt-C)	0.00	0.01	0.00	0.01	0.00	0.02	0.60
Fe	−1.75	1.854 (Fe-C)	**−0.20**	2.62	0.08	2.62	**0.10**	2.62	3.09
Co	−1.45	1.833 (Co-C)	**1.05**	1.32	**0.19**	1.33	0.12	1.33	1.76
Ru	−1.93	1.985 (Ru-C)	−2.53	1.09	0.12	1.07	0.12	1.08	1.12
Pt_2Fe	−1.44	1.872 (Fe-C)	**−1.79**	1.11	0.06	1.12	**0.07**	1.13	1.33
PtFe	−1.70	1.873 (Fe-C)	**−0.46**	1.52	0.07	1.53	**0.10**	1.52	2.36
$PtFe_2$	−1.34	1.866 (Fe-C)	**−1.10**	1.95	0.06	1.95	**0.08**	1.95	2.67
Pt_2Co	−1.50	1.842 (Co-C)	**0.80**	0.59	**0.12**	0.59	0.06	0.64	1.03
PtCo	−1.69	1.833 (Co-C)	**0.24**	0.78	**0.14**	0.79	0.08	0.79	1.56
$PtCo_2$	−1.73	1.849 (Co-C)	**0.90**	0.99	**0.18**	0.99	0.08	0.98	1.87
Pt_2Ru	−1.62	1.961 (Ru-C)	−0.73	0.64	0.10	0.64	0.04	0.67	1.10
PtRu	−1.99	1.956 (Ru-C)	**3.53**	0.64	**0.17**	0.62	0.04	0.60	0.83
$PtRu_2$	−1.80	1.963 (Ru-C)	−2.39	1.07	0.10	1.07	0.07	1.10	1.10

[a]Only the shortest BD is listed with the specific bond in parentheses.

[b]$\mu_{S\|\|}$ and $\mu_{S\perp}$ denote the calculated spin-magnetic moment with the magnetization directions to be parallel and perpendicular to the tube axis, respectively; while $\mu_{L\|\|}$ and $\mu_{L\perp}$ are the corresponding orbital-magnetic moments, respectively. The $\mu_{S\perp}$ and $\mu_{L\perp}$ are defined as a vector sum of contributions from the x and y directions, as shown in Fig. 1. The calculated magnetic moments (based on an atomic-sphere approximation) for a freestanding monatomic TM-alloy string and a TM-alloy-string/B-CNT are listed as μ_0 and μ, respectively. The MAEs corresponding to the largest μ_L are highlighted in bold.

for our composite systems by including SOC effects. The MAE for a magnetic system mainly arises from the magnetocrystalline anisotropy (known also as the electronic contribution), originating from the orbital magnetization and SOC effects, which are captured using noncollinear DFT calculations. It is known that a sizable MAE arises from large spin- and orbital-magnetic moments and a strong SOC. Large spin moments can be found among the ferromagnetic 3*d* metals Fe and Co, as well as 4*d* metal Ru, but unfortunately, these metals have small orbital moments and SOC effects are thus weak. In general, strong SOC can be found in the heavy 5*d* metals, e.g., Pt, which however is nonmagnetic. Monatomic chains of Pt alloys with varied composition of Fe, Co, and Ru may lead to tunable MAE and spin- and orbital-moments.

As shown in Fig. 3, the TDOS at the Fermi level (E_F) of our systems are spin polarized and this is mainly attributed to the spin-down *d* states of the alloying elements. The spin-up *d* states of Fe, Co, and Ru are nearly completely filled below E_F, resulting in a small or negligible PDOS at E_F. In contrast, the spin-down *d* states are only partially occupied, resulting in a large PDOS at E_F. The *d* states of Pd contribute little to the spin-polarized states of the system, as seen from their location (i.e., below E_F). In particular, the PtCo-string/B-CNT composite acts as a half-metal, which is a conductor to electrons with a spin-down orientation but an insulator to electrons with a spin-up orientation, as shown in Fig. 3(e). Therefore, the magnetic properties of our systems are mainly controlled by the magnetic alloying element (i.e., Fe, Co, and Ru).

A previous study reported that free and deposited Pt monatomic chains have increasingly larger magnetic moments (μ_0=0.36–0.95μ_B/Pt atom) and stronger magnetic anisotropy as the interatomic distance is increased, especially beyond the equilibrium interatomic distance.[11] Our recent studies have shown that a Pt-string/B-CNT model is nearly nonmagnetic (μ_0=0.60 and μ=0.018μ_B/Pt atom).[38] As shown in Table I, as the alloying-element composition is increased, the magnetic moment for the Pt-alloy-string/B-CNT is also increased: Pt_2Fe (1.13μ_B/TM atom), PtFe (1.52μ_B/TM atom), and $PtFe_2$ (1.95μ_B/TM atom). Thus, the nonmagnetic Pt-string/B-CNT can be tuned to be magnetic by alloying with magnetic elements, such as Fe, Co, and Ru. Considering that spin-current transports are mainly determined by the electron channel across E_F, our calculated results suggest that alloying, which is commonly used in bulk materials to enhance their electrical and magnetic properties, can also be applied to nanomaterials for tailoring their spin-polarized properties.

Moreover, one can see that spin- and orbital-magnetic moments of the Pt alloy systems along the magnetization directions can be tuned by changing the alloy component and the composition (Table I). This mainly arises from the interactions of the 5*d* states of Pt with the 3*d* states of Fe and Co [see Figs. 3(a)–3(f)] and the 4*d* states of Ru [see Figs. 3(g)–3(i)]. Interestingly, the easy axes for the Pt-alloy/B-CNT systems are generally in accordance with those of the alloy component in the system (i.e., Fe, Co, and Ru). As shown in Table I, the MAEs for the Pt-Fe alloy systems are negative, which indicates perpendicular easy magnetization axes. This corresponds with the perpendicular direction of maximum orbital moments (i.e., μ_L). The negative MAEs could be induced by Fe in the systems, which also have negative MAEs. Similar cases can also be found for the Pt-Co and for the Pt-Ru systems. In Table II, we also list the spin- and orbital-magnetic moments (in μ_B) for each TM atom in Pt-Fe/B-CNT systems when the magnetization direc-

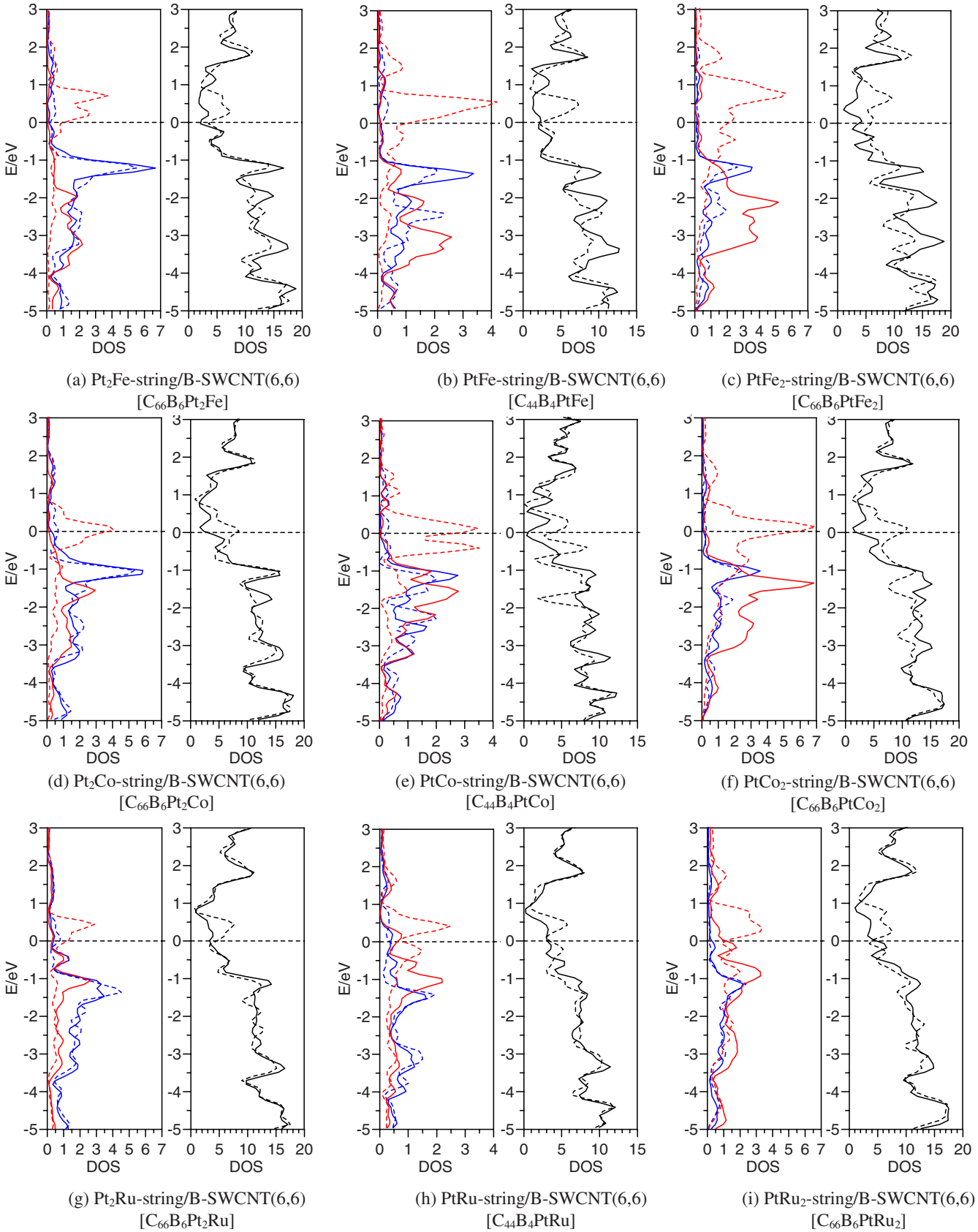

(a) Pt_2Fe-string/B-SWCNT(6,6) $[C_{66}B_6Pt_2Fe]$

(b) PtFe-string/B-SWCNT(6,6) $[C_{44}B_4PtFe]$

(c) $PtFe_2$-string/B-SWCNT(6,6) $[C_{66}B_6PtFe_2]$

(d) Pt_2Co-string/B-SWCNT(6,6) $[C_{66}B_6Pt_2Co]$

(e) PtCo-string/B-SWCNT(6,6) $[C_{44}B_4PtCo]$

(f) $PtCo_2$-string/B-SWCNT(6,6) $[C_{66}B_6PtCo_2]$

(g) Pt_2Ru-string/B-SWCNT(6,6) $[C_{66}B_6Pt_2Ru]$

(h) PtRu-string/B-SWCNT(6,6) $[C_{44}B_4PtRu]$

(i) $PtRu_2$-string/B-SWCNT(6,6) $[C_{66}B_6PtRu_2]$

FIG. 3. (Color online) Calculated TDOS (right) and PDOS (left) for TM-alloy-string/B-SWCNT(6,6) composites of one supercell with the composition included in brackets. The solid and dashed lines represent spin-up and spin-down states, respectively. Black, blue, and red lines represent TDOS, PDOS for the *d*-states of Pt, and the *d* states of the other TMs (i.e., Ru, Fe, and Co), respectively. The Fermi level (horizontal black dashed line) is shifted to zero eV.

TABLE II. The spin- and orbital-magnetic moments (in μ_B) for the transition-metal atoms in the monatomic chain/B-CNT systems when the magnetization directions are along x[100], y[010], and z[001], respectively, as shown in Fig. 1. All of the values for the Pt_3/B-CNT system are essentially zero (hence, not shown). The maximum spin- and orbital-magnetic moments are shown in a bold font.

(a) Pt_2Fe/B-CNT

	x[100]			Y[010]			z[001]		
	S_x	S_y	S_z	S_x	S_y	S_z	S_x	S_y	S_z
Pt_1	**0.16**	0.00	0.00	0.01	**0.16**	0.00	0.00	0.00	**0.15**
Pt_2	**0.14**	0.00	0.00	0.00	**0.15**	0.00	0.00	0.00	**0.14**
Fe_3	**2.79**	−0.02	0.00	0.01	**2.79**	0.01	0.00	−0.01	**2.78**
	L_x	L_y	L_z	L_x	L_y	L_z	L_x	L_y	L_z
Pt_1	**0.03**	0.03	−0.01	0.03	**0.07**	0.00	−0.01	0.00	**0.04**
Pt_2	**0.02**	0.03	0.00	0.03	**0.06**	0.00	0.01	0.00	**0.04**
Fe_3	**0.06**	0.03	0.00	0.03	**0.07**	−0.01	−0.01	0.00	**0.09**

(b) PtFe/B-CNT

	x[100]			y[010]			z[001]		
	S_x	S_y	S_z	S_x	S_y	S_z	S_x	S_y	S_z
Pt_1	**0.16**	0.00	0.00	0.00	**0.16**	0.00	0.00	0.00	**0.16**
Fe_2	**2.79**	0.00	0.00	0.00	**2.79**	0.00	0.00	0.00	**2.79**
	L_x	L_y	L_z	L_x	L_y	L_z	L_x	L_y	L_z
Pt_1	**0.04**	0.02	0.00	0.02	**0.09**	0.00	0.00	0.00	**0.05**
Fe_2	**0.04**	0.02	0.00	0.03	**0.10**	0.00	0.00	0.00	**0.09**

(c) $PtFe_2$/B-CNT

	x[100]			y[010]			z[001]		
	S_x	S_y	S_z	S_x	S_y	S_z	S_x	S_y	S_z
Pt_1	**0.11**	0.01	0.00	0.00	**0.12**	0.00	0.00	0.00	**0.11**
Fe_2	**2.61**	0.00	0.00	0.01	**2.61**	0.00	0.00	0.01	**2.61**
Fe_3	**2.62**	0.00	0.00	−0.01	**2.63**	0.00	0.00	−0.01	**2.63**
	L_x	L_y	L_z	L_x	L_y	L_z	L_x	L_y	L_z
Pt_1	**0.02**	0.02	0.00	0.01	**0.06**	0.00	0.00	0.00	**0.03**
Fe_2	**0.04**	0.01	−0.01	0.02	**0.09**	−0.01	−0.01	0.01	**0.07**
Fe_3	**0.04**	0.01	0.01	0.03	**0.09**	0.01	0.01	−0.01	**0.07**

(d) Fe_3/B-CNT

	x[100]			y[010]			z[001]		
	S_x	S_y	S_z	S_x	S_y	S_z	S_x	S_y	S_z
Fe_1	**2.41**	0.00	0.00	0.00	**2.41**	0.00	0.00	0.00	**2.41**
Fe_2	**2.41**	0.00	0.00	0.00	**2.41**	0.00	0.00	0.00	**2.42**
Fe_3	**2.41**	0.00	0.00	0.00	**2.41**	0.00	0.00	0.00	**2.41**
	L_x	L_y	L_z	L_x	L_y	L_z	L_x	L_y	L_z
Fe_1	**0.05**	0.01	0.00	0.01	**0.10**	0.00	0.00	0.00	**0.08**
Fe_2	**0.05**	0.01	0.00	0.01	**0.10**	0.00	−0.01	0.00	**0.08**
Fe_3	**0.05**	0.01	0.00	0.01	**0.10**	0.00	0.01	0.00	**0.08**

tions are along x[100], y[010], and z[001], respectively, as shown in Fig. 1. One can see that the maximum orbital-magnetic moments for every TM atom are parallel to their spin-magnetic moments.

We also found that the SOC effects are mainly contributed from the d-electron spin- and orbital-magnetic moments of the alloying atoms, which, in general, have sizable μ_S and μ_L. The Pt atoms in the Pt-alloy-string/B-CNT systems have much smaller μ_S but comparable μ_L (see Table II). Despite the strong bonding interactions mentioned above, the sizable spin- and orbital-magnetic moments survive for both magnetization directions ($\mu_{L\parallel}$ and $\mu_{L\perp}$). There is the notion that the energy induced by SOC can be assumed to be proportional to the projection of the spin on the orbital momentum, leading to an easy magnetization axis in the direction of maximum orbital moment. Indeed, most of the Pt-alloy-string/B-CNT systems agree with this notion (highlighted in bold in Table I). However, exceptions were found for the Pt-Ru alloy system. One can see that the orbital momentum $\mu_{L\parallel}$ is larger than $\mu_{L\perp}$. However, their MAEs (except PtRu-string/B-CNT) are negative, suggesting the perpendicular easy axis. It has been experimentally observed that the maximum orbital moments are not *always* obtained along the easy axis under the influence of ligand states.[53]

Our calculations suggest that by changing the composition of the Pt-alloy, the easy axis of the Pt-alloy/B-CNT can oscillate between the magnetization directions parallel to and orthogonal to the tube axis. In fact, previous theoretical studies[34,35] have predicted that the MAE of Fe and Co nanowires oscillates with respect to chain width and depends strongly on the transversal structure. The oscillatory magnetic anisotropy in 1D Co atomic wires grown on Pt(997) has also been experimentally observed by x-ray magnetic circular dichroism.[5] Furthermore, several theoretical studies[11,21,23,31–35] have predicted that TM monatomic chains (e.g., Fe, Co, and Pt), have an easy magnetization axis changed from the direction parallel to the wire axis to that perpendicular to the wire axis after they are deposited on a Pt or Pd substrate, suggesting the importance of the substrate on the magnetic anisotropy. Here, our calculated results further confirm the impact of the alloying element on the magnetic anisotropy.

IV. CONCLUSIONS

Our calculations show that B-CNT-templated Pt-alloy nanostructures, like their pure TM counterparts, demonstrate strong molecular recognition, leading to the self-assembly of Pt-alloy monatomic chains having well-defined covalent bonds with the substrate. The density of states of our systems at the Fermi level (E_F) are spin polarized, which are mainly controlled by the spin-down d states of the alloying element (i.e., Fe, Co, and Ru). The easy axes for the Pt-alloy/B-CNT systems are generally determined by those of the alloy component in the systems (i.e., Fe, Co, and Ru). By changing the composition and component of the Pt alloy, the easy axis of the composite material can oscillate between the magnetization directions parallel to and perpendicular to the tube axis. Our calculations also suggest that the TM-alloy strings anchored on a B-CNT substrate via strong molecular interactions (i.e., chemical bonds) could still possess magnetic anisotropy with sizable MAE. The high stability and interesting electronic and magnetic features could render these Pt-alloy-string/B-CNT composites useful in a wide variety of next-generation device components.

ACKNOWLEDGMENTS

The authors appreciate helpful discussions with Claudia Mewes and Bill Butler about the calculation details. Funding for this work has been provided by an NSF CAREER Award (No. 0747690). Supercomputer resources were provided by the Alabama Supercomputer Center, the NCSA TeraGrid, and the Pacific Northwest National Laboratory EMSL facility.

*Corresponding author; hturner@eng.ua.edu

[1] R. H. Baughman, A. A. Zakhidov, and W. A. de Heer, Science **297**, 787 (2002).
[2] J. Robertson, Mater. Today **10**, 36 (2007).
[3] A. Javey, ACS Nano **2**, 1329 (2008).
[4] P. Gambardella, A. Dallmeyer, K. Maiti, M. C. Malagoli, W. Eberhardt, K. Kern, and C. Carbone, Nature (London) **416**, 301 (2002).
[5] P. Gambardella, A. Dallmeyer, K. Maiti, M. C. Malagoli, S. Rusponi, P. Ohresser, W. Eberhardt, C. Carbone, and K. Kern, Phys. Rev. Lett. **93**, 077203 (2004).
[6] H. Fujisawa, S. Shiraki, M. Furukawa, S. Ito, T. Nakamura, T. Muro, M. Nantoh, and M. Kawai, Phys. Rev. B **75**, 245423 (2007).
[7] A. Dallmeyer, C. Carbone, W. Eberhardt, C. Pampuch, O. Rader, W. Gudat, P. Gambardella, and K. Kern, Phys. Rev. B **61**, R5133 (2000).
[8] V. Rodrigues, J. Bettini, P. C. Silva, and D. Ugarte, Phys. Rev. Lett. **91**, 096801 (2003).
[9] A. Vindigni, A. Rettori, M. G. Pini, C. Carbone, and P. Gambardella, Appl. Phys. A: Mater. Sci. Process. **82**, 385 (2006).
[10] J. Velev, R. F. Sabirianov, S. S. Jaswal, and E. Y. Tsymbal, Phys. Rev. Lett. **94**, 127203 (2005).
[11] A. Smogunov, A. Dal Corso, A. Delin, R. Weht, and E. Tosatti, Nat. Nanotechnol. **3**, 22 (2008).
[12] A. Smogunov, A. Dal Corso, and E. Tosatti, Phys. Rev. B **78**, 014423 (2008).
[13] Y. Mokrousov, G. Bihlmayer, S. Heinze, and S. Blugel, Phys. Rev. Lett. **96**, 147201 (2006).
[14] Y. Mokrousov, G. Bihlmayer, S. Blugel, and S. Heinze, Phys. Rev. B **75**, 104413 (2007).
[15] A. Delin and E. Tosatti, J. Phys.: Condens. Matter **16**, 8061 (2004).
[16] A. Delin and E. Tosatti, Phys. Rev. B **68**, 144434 (2003).

[17] A. Delin, E. Tosatti, and R. Weht, Phys. Rev. Lett. **92**, 057201 (2004).
[18] G. Autès, C. Barreteau, D. Spanjaard, and M. C. Desjonqueres, J. Phys.: Condens. Matter **18**, 6785 (2006).
[19] Y. Li and B. G. Liu, Phys. Rev. B **73**, 174418 (2006).
[20] L. He, D. S. Kong, and C. P. Chen, J. Phys.: Condens. Matter **19**, 446207 (2007).
[21] M. Komelj, D. Steiauf, and M. Fahnle, Phys. Rev. B **73**, 134428 (2006).
[22] A. B. Shick, F. Maca, J. Masek, and T. Jungwirth, Phys. Rev. B **73**, 024418 (2006).
[23] A. B. Shick, F. Maca, and P. M. Oppeneer, Phys. Rev. B **69**, 212410 (2004).
[24] A. B. Shick, F. Maca, and P. M. Oppeneer, J. Magn. Magn. Mater. **290-291**, 257 (2005).
[25] R. A. Guirado-López, J. M. Montejano-Carrizalez, and J. L. Moran-Lopez, Phys. Rev. B **77**, 134431 (2008).
[26] R. Félix-Medina, J. Dorantes-Davila, and G. M. Pastor, New J. Phys. **4**, 100 (2002).
[27] Z. Šljivančanin, Z. S. Popovic, F. R. Vukajlovic, and A. Baldereschi, Phys. Rev. B **74**, 134412 (2006).
[28] J. C. Tung and G. Y. Guo, Phys. Rev. B **76**, 094413 (2007).
[29] C. Ataca, S. Cahangirov, E. Durgun, Y. R. Jang, and S. Ciraci, Phys. Rev. B **77**, 214413 (2008).
[30] S. R. Bahn and K. W. Jacobsen, Phys. Rev. Lett. **87**, 266101 (2001).
[31] B. Lazarovits, L. Szunyogh, and P. Weinberger, Phys. Rev. B **67**, 024415 (2003).
[32] B. Lazarovits, L. Szunyogh, and P. Weinberger, J. Magn. Magn. Mater. **272-276**, 1658 (2004).
[33] B. Lazarovits, L. Szunyogh, P. Weinberger, and B. Ujfalussy, Phys. Rev. B **68**, 024433 (2003).
[34] J. Dorantes-Dávila and G. M. Pastor, Phys. Rev. Lett. **81**, 208 (1998).
[35] J. Dorantes-Dávila and G. M. Pastor, Phys. Rev. B **72**, 085427 (2005).
[36] L. Fernández-Seivane, V. M. Garcia-Suarez, and J. Ferrer, Phys. Rev. B **75**, 075415 (2007).
[37] B. Újfalussy, B. Lazarovits, L. Szunyogh, G. M. Stocks, and P. Weinberger, Phys. Rev. B **70**, 100404 (2004).
[38] W. An and C. H. Turner, J. Phys. Chem. C **113**, 15346 (2009).
[39] W. T. Geng and K. S. Kim, Phys. Rev. B **67**, 233403 (2003).
[40] J. Bettini, F. Sato, P. Z. Coura, S. O. Dantas, D. S. Galvao, and D. Ugarte, Nat. Nanotechnol. **1**, 182 (2006).
[41] W. Fa and J. M. Dong, J. Chem. Phys. **128**, 244703 (2008).
[42] A. Enomoto, S. Kurokawa, and A. Sakai, Phys. Rev. B **65**, 125410 (2002).
[43] Abu Md. Asaduzzaman and M. Springborg, Phys. Rev. B **72**, 165422 (2005).
[44] G. Kresse and J. Furthmuller, Comput. Mater. Sci. **6**, 15 (1996).
[45] D. Hobbs, G. Kresse, and J. Hafner, Phys. Rev. B **62**, 11556 (2000).
[46] W. An and C. H. Turner, J. Phys. Chem. C **113**, 7069 (2009).
[47] P. E. Blöchl, O. Jepsen, and O. K. Andersen, Phys. Rev. B **49**, 16223 (1994).
[48] J. P. Perdew, K. Burke, and M. Ernzerhof, Phys. Rev. Lett. **77**, 3865 (1996).
[49] M. Methfessel and A. T. Paxton, Phys. Rev. B **40**, 3616 (1989).
[50] P. Bloński and J. Hafner, J. Phys.: Condens. Matter **21**, 426001 (2009).
[51] O. Stephan, P. M. Ajayan, C. Colliex, P. Redlich, J. M. Lambert, P. Bernier, and P. Lefin, Science **266**, 1683 (1994).
[52] W. Q. Han, Y. Bando, K. Kurashima, and T. Sato, Chem. Phys. Lett. **299**, 368 (1999).
[53] C. Andersson, B. Sanyal, O. Eriksson, L. Nordstrom, O. Karis, D. Arvanitis, T. Konishi, E. Holub-Krappe, and J. H. Dunn, Phys. Rev. Lett. **99**, 177207 (2007).